Journal of Chromatography A, 1217 (2010) 1320–1331

Contents lists available at ScienceDirect

Journal of Chromatography A

journal homepage: www.elsevier.com/locate/chroma

On the enantioselectivity of the mass transfer kinetics and the adsorption equilibrium of Naproxen on the chiral stationary phase (*R*, *R*)-Whelk-O1 under reversed-phase conditions

Leonid Asnin[a,b], Krisztián Horváth[b,c], Georges Guiochon[b,*]

[a] *Institute of Technical Chemistry, The Ural Branch, of the Russian Academy of Sciences, Perm 614013, Russia*
[b] *Department of Chemistry, University of Tennessee, Knoxville, TN 37996-1600, USA*
[c] *Department of Analytical Chemistry, University of Pannonia, P.O. Box 158, Veszprém H-8200, Hungary*

ARTICLE INFO

Article history:
Received 13 October 2009
Received in revised form
16 December 2009
Accepted 21 December 2009
Available online 4 January 2010

Keywords:
Chiral separations
Naproxen
Whelk-O1
Pirkle phases

ABSTRACT

The adsorption of the Naproxen enantiomers on a Pirkle-type chiral stationary phase (CSP) (*R*, *R*)-Whelk-O1 from 0.01 M acetic acid solution in a methanol–water (85/15, v/v) mixture was studied using techniques of frontal analysis and elution chromatography. Adsorption was found to follow a model that assumes retention of a solute on two types of surface sites, enantioselective and nonselective. Some minor deviations from the classical bi-Langmuir model were found, but they were well accounted for by assuming the coexistence of two groups of enantioselective sites: sparse sites of strong affinity toward (*R*)-Naproxen and a more numerous type of low-energy sites exhibiting a somewhat different affinity toward the two enantiomers. Special consideration is paid to the adsorption of the methanol–water mixture on the surface of the CSP. The bonded organic layer exhibits hydrophobic properties, so the adsorbed layer is enriched in methanol throughout the whole range of mobile phase compositions. The study of the mass transfer kinetics was carried out by analyzing the dependence of the HETP on the flow velocity. It revealed the enantioselective character of the intraparticle transport processes. Other aspects of the column dynamics, such as axial dispersion, the external and internal mass transfer were also discussed.

1. Introduction

The resolution of the Naproxen enantiomers (Fig. 1) on a Whelk-O1 chiral stationary phase (CSP) (Fig. 2) [1,2] is the most prominent example of direct chromatographic enantioseparation. Since its publication in 1992 [1], it has been abundantly cited in numerous reviews and has become an obligatory part of chapters and treatises on chiral separations. It illustrates the potential of chiral chromatography to solve complicated separation problems, like the direct resolution of the racemates of underivatized acids. It is also one of the most successful demonstrations of a rational approach for the design of chiral selectors that has since then become an important tool in the development of CSPs [2]. The nature of the enantiodiscrimination between the Naproxen enantiomers by the Whelk-O1 chiral selector was comprehensively studied [3–9]. However, the macroscopic mechanisms of adsorption of Naproxen on this CSP remain unclear. Apparently, only a recent publication [10] discusses the adsorption isotherms of the Naproxen enantiomers on this CSP while there are no data on their mass transfer kinetics.

The main goal of this work is to fill in the gaps in our knowledge of the equilibrium and the dynamics of adsorption on this important Pirkle-type phase. The work was carried out under reversed-phase conditions (with a methanol–water mobile phase). This choice was dictated by a requirement of a high solubility of the analyte in the mobile phase, which is necessary for the measurement of adsorption isotherms over a wide concentration range. Besides, the application of Whelk-O1 in the reversed-phase mode has been poorly covered. A few examples of the use of this CSP with water-containing mobile phases have been previously reported [11–13]. The retention of several chiral analytes in reversed-phase liquid chromatography and in the so-called polar organic mode were studied using a linear chromatography method [14,15]. Therefore the extension of investigations involving aqueous solutions is of separate interest.

* Corresponding author. Fax: +1 865 974 2667.
E-mail address: guiochon@utk.edu (G. Guiochon).

0021-9673/$ – see front matter © 2009 Elsevier B.V. All rights reserved.
doi:10.1016/j.chroma.2009.12.066

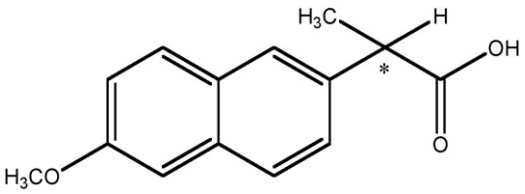

Fig. 1. Structure of Naproxen. Symbol "star" shows the location of the chiral center.

2. Theory

2.1. The concepts of excess and total adsorption

The two definitions of the adsorbed amount, excess and total amounts adsorbed, are used in this work. A detailed description of those concepts can be found in Refs. [16,17]. Only a brief summary useful for the subsequent discussion is given. The excess amount adsorbed is defined as the excess of solute contained in the adsorption system compared to what would be contained in a hypothetical system in which the solute concentration is uniform throughout the whole volume of mobile phase and equal to the equilibrium concentration in the bulk phase of the real system [17]. This value is directly measured in an adsorption experiment. The measurement does not require any prior knowledge of the size, structure, and properties of the actual adsorbed phase, in contrast to the value of the total adsorbed amount, which is defined as the amount of solute contained in an adsorbed layer of finite thickness [18].

The operational definition of the excess adsorbed amount adopted in this work relies on the assumption of a constant total volume of the liquid phase in the system, V_0 [16]:

$$\Gamma_i = \frac{(c_{0,i} - c_i)V_0}{V_a} \tag{1}$$

where $c_{0,i}$ and c_i are the concentrations of the component i before and after the equilibrium is established, and V_a is the stationary phase volume.

The expression determining the total adsorption reads

$$q_i = \frac{g\,S}{V_a} c_i \delta + \Gamma_i(c_i) \tag{2}$$

where g is the mass of adsorbent, S its specific surface area, and δ the thickness of the adsorbed layer. Since there are no experimental methods able to determine the analyte distribution in the direction normal to the surface, the assignment of δ relies on a conceptual model of the structure of the adsorbed phase, which is generally arbitrary. Note that for solutions of solids, it is almost always safe to assume that the excess adsorption is equal to the total adsorbed amount, because the solute concentration is restricted by the solubility of the solid, which is generally low enough for the term $(gS/V_a)c\delta$ to be negligible compared to Γ.

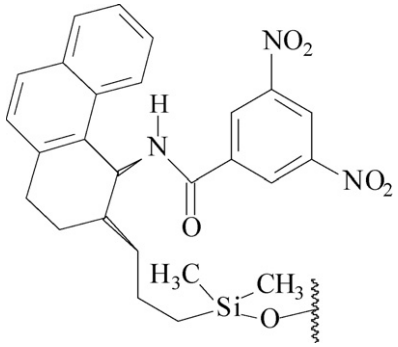

Fig. 2. Structure of the (*R,R*)-Whelk-O1 chiral selector.

2.2. Total adsorption isotherm models

The concept of total adsorption allows the use of an approach based on the law of mass action to studies of liquid/solid equilibria. In the framework of this approach, a number of adsorption isotherm models were developed, including the well-known Langmuir isotherm. This model supposes that there exists on the surface of an adsorbent a finite number of adsorption sites of equal affinity toward a certain compound, the adsorbate. Let $q^\star$ be the concentration of these adsorption sites and b be the adsorption equilibrium constant or adsorption coefficient. Then the isotherm equation reads

$$q = \frac{q^\star bc}{1 + bc} \tag{3}$$

In chiral chromatography, an adsorption model is often considered, in which two types of adsorption sites coexist on the stationary phase, the enantioselective and the nonselective sites. These sites are assumed to interact independently with a chiral analyte [19,20]. The enantioselective sites exhibit different affinities toward the two enantiomers whereas the nonselective sites interact with both antipodes identically. The adsorption isotherm for this model (the so-called bi-Langmuir isotherm) is merely the sum of two Langmuir terms, one for each types of adsorption sites:

$$q = \frac{q^\star_{ns} b_{ns} c}{1 + b_{ns} c} + \frac{q^\star_s b_s c}{1 + b_s c} \tag{4}$$

The indices *ns* and *s* correspond to the nonselective and the selective adsorption sites, respectively. It is obvious that for the enantiomers (*R*) and (*S*), the following conditions are true:

$$b_{ns,R} = b_{ns,S} = b_{ns} \qquad \text{and} \qquad b_{s,S} \neq b_{s,R} \tag{5}$$

The equilibrium adsorption constants at infinite dilution (Henry coefficient, K_H) for this isotherm is given by the expression [19]:

$$K_H = q^\star_{ns} b_{ns} + q^\star_s b_s \tag{6}$$

where b_s is different for both enantiomers while $q^\star_s$, $q^\star_{ns}$, and b_{ns} are identical.

2.3. Mass transfer kinetics

During its migration through a bed of an adsorbent, a solute band broadens due to the influence of two factors: a thermodynamic and a kinetic one. Under linear conditions, only kinetic phenomena cause broadening of chromatographic bands [21]. Therefore the measurements of the peak dispersion of strongly diluted samples provide information on kinetic processes in a chromatographic column. In general, one considers four mechanisms of kinetic band broadening: axial dispersion, the external film mass transfer resistance, intraparticle diffusion, and the rate of adsorption–desorption. The general rate (GR) model of column dynamics takes into account all these mechanisms [21]. The model assumes that (1) the mobile phase percolates through the interstitial volume between stationary phase particles while it is stagnant in the particles; (2) that solute molecules diffuse from the flowing stream to the stagnant mobile phase and across it; and (3) that adsorption–desorption takes place between the stagnant mobile phase within the pores and the adsorbent surface. The set of mass balance and kinetic equations describing the GR model cannot be solved analytically in time domain. However, there exists a solution in the Laplace domain, from which the statistical moments of the band profiles are readily derived [21].

By definition, the first moment (μ_1) and the second central moment (μ'_2) of chromatographic peaks are

$$\mu_1 = \frac{\int c(V)V\mathrm{d}V}{\int c(V)\mathrm{d}V} \tag{7}$$

$$\mu'_2 = \frac{\int c(V)(V-\mu_1)^2\mathrm{d}V}{\int c(V)\mathrm{d}V} \tag{8}$$

where V is the retention volume.

The theoretical plate number (N) of a column is the ratio μ_1^2/μ'_2, so this ratio provides the height equivalent to a theoretical plate (HETP), $H = L/N$, with L the column length, a fundamental characteristic of chromatographic band dispersion. In the framework of the GR model the HETP relates to several dynamic coefficients through the following equation [21]:

$$H = \frac{2D_{ax}}{u} + 2u\left(\frac{k_1}{1+k_1}\right)^2\left[\frac{d_p^2}{60F_eD_p} + \frac{d_p}{6F_ek_f} + \left(\frac{k_p}{1+k_p}\right)^2\frac{1}{F_ek_{ads}}\right] \tag{9}$$

with

$$F_e = \frac{1-\epsilon_e}{\epsilon_e} \tag{10}$$

$$k_1 = F_e(\epsilon_i + (1-\epsilon_i)K_H) \tag{11}$$

$$k_p = \frac{1-\epsilon_i}{\epsilon_i}K_H \tag{12}$$

where u is the interstitial linear velocity of the mobile phase, d_p the particle diameter, D_{ax} the axial dispersion coefficient, D_p the intraparticle diffusivity, k_f the external mass transfer coefficient, k_{ads} the adsorption rate constant, and ϵ_e and ϵ_i are the external and internal porosity of the column, respectively. All the contributions to band broadening due to kinetic factors, except axial dispersion are proportional to u. Consequently, the analysis of the H *vs.* u plots delivers merely a lumped coefficient for the sum of the linear terms of Eq. (9). Deconvoluting information concerning the individual kinetic processes from this coefficient is a task that is beyond the possibilities of chromatographic experiments. It must rely on some extra-chromatographic correlations.

The complexity of the axial dispersion coefficient was comprehensively discussed by Giddings [22]. According to the classical approach, it results from the addition of the contributions of two main mechanisms, molecular diffusion in the bed voids and eddy diffusion. Hence the expression for the D_{ax} can be written as [21]:

$$D_{ax} = \gamma_1 D_m + \gamma_2 d_p u \tag{13}$$

where D_m is the molecular diffusivity, and γ_1 and γ_2 are geometrical parameters. Giddings has argued with this additive scheme, suggesting a coupling effect between the flow velocity and the radial diffusion in the void space of the packing [22]. According to this concept, the resistances to axial diffusion are additive but not the diffusivities themselves. Consequently, the contribution of eddy diffusion to the HETP equation taking into account the coupling effect reads

$$H_{cpl} = \frac{1}{1/(\lambda_1 d_p) + D_m/(\lambda_2 d_p^2 u)} \tag{14}$$

Combining Eqs. (13),(14) with the HETP equation, one obtains the van Deemter (15) or the Giddings (16) equation:

$$H = A + \frac{B}{u} + Cu \tag{15}$$

$$H = \frac{1}{1/a + 1/(bu)} + \frac{B}{u} + Cu \tag{16}$$

where the parameters A and B describe the effect of eddy and molecular diffusion, respectively, and the parameters a and b describe the contribution of eddy and molecular diffusion in the coupling effect. The parameter C accounts for the constant part of the second term of the right hand side of Eq. (9).

2.3.1. Empirical correlations for the dynamic parameters

As above mentioned, a chromatographic experiment gives a lumped coefficient of mass transfer. The assessment of the partial contributions of each of the different kinetic processes to the overall band broadening requires the independent determination of the corresponding kinetic coefficients. In the literature, different empirical correlations are found that allow the derivation of some of these dynamic parameters.

2.3.1.1. The molecular diffusion coefficient. The molecular diffusivity of naproxen was derived from the Wilke-Chang equation [23]:

$$D_m = 7.4\times10^{-8}\frac{(\overline{\phi M})^{0.5}T}{\eta V_b^{0.6}} \tag{17}$$

where T is the temperature, η the viscosity of the mobile phase, $(\overline{\phi M}) = \sum_i x_i\phi_i M_i$ (i = methanol, water) is a correction allowing for the influence of hydrogen bonding on molecular diffusion, x is the mole fraction of the organic modifier in the mixed solvent, M_i the molecular mass of the mobile phase component i, ϕ the association coefficient, 1.9 and 2.6 for methanol and water, respectively, and V_b is the molar volume of the solute at its boiling point. This last parameter was estimated with the help of the Le Bas increment method as recommended in [23].

2.3.1.2. The external mass transfer coefficient. There are several empirical correlations proposed to predict the coefficient of external mass transfer, k_f, at low Reynolds number. The most popular is the Wilson-Geankoplis equation [24], which is valid in the range of $0.0015 < Re < 55$:

$$k_f = 1.09\left(\frac{D_m}{d_p}\right)^{2/3}u^{1/3}\epsilon_e^{2/3} \tag{18}$$

where $Re = u\epsilon_e d_p\rho/\eta$ is the Reynolds number (ρ is the density of the mobile phase).

Alternately, the Kataoka correlation [21] can be applied for $Re < 100$:

$$k_f = 1.85\left(\frac{D_m}{d_p}\right)^{2/3}u^{1/3}(1-\epsilon_e)^{1/3} \tag{19}$$

The value of the external mass transfer coefficient can also be found based on the penetration theory [25], which provides the following equation for k_f:

$$k_f = \sqrt{\frac{4D_m u}{\pi d_p}} \tag{20}$$

2.3.1.3. Intraparticle pore diffusivity. The coefficient of diffusion in the internal pore volume of the particles, given that intraparticle convection [26] is negligible, correlates to the molecular diffusivity through a general expression $D_p = (\epsilon_i D_m)/\tau$, where τ is the tortuosity factor, which accounts for the tortuosity and the constriction of the pore network in the particles. Its *a priory* evaluation heavily depends on the model of porous structure assumed for the particles. Different models are found in the literature [27,28]. They are all oversimplifications of real porous solids. Besides, frequently, the structure of the pore space is unknown and it is extremely difficult to determine a geometrical representation of it. It is unclear which model should be preferred.

We elected to choose the model that is most often accepted under similar conditions. In liquid chromatography, the model of Mackie and Mears [29] is widely used. This model gives the following equation for pore diffusivity:

$$D_p = \left(\frac{\epsilon_i}{2-\epsilon_i}\right)^2 D_m \tag{21}$$

2.3.1.4. The axial dispersion coefficient. In the present study, the apparent D_{ax} value derived from the experimental data was used in the calculations. Nevertheless, it is useful for the sake of comparison to estimate this value by an empirical correlation. In liquid chromatography a correlation given by Gunn [30] is used frequently:

$$\frac{D_{ax}}{d_p u} = G_1 + G_2 + \frac{\epsilon_e}{1.4 Re\, Sc} \tag{22}$$

with

$$G_1 = \frac{Re\, Sc}{4j_1^2(1-\epsilon_e)}(1-p)^2 \tag{23}$$

$$G_2 = \frac{(Re\, Sc)^2}{14 j_1^4 (1-\epsilon_e)^2} p(1-p)^3 \left[\exp\left(\frac{-4j_1^2(1-\epsilon_e)}{p(1-p)Re\, Sc}\right) - 1\right] \tag{24}$$

where $Sc = \eta/(\rho D_m)$ is the Schmidt number, $j_1 = 2.405$ is the first root of zero-order Bessel function, and $p = 0.17 + 0.33\exp(-24/Re)$.

3. Experimental

3.1. Apparatus

All experiments were carried out using a HP 1090 Series II liquid chromatograph (Hewlett Packard, now Agilent Technologies, Palo Alto, CA), equipped with a multi-solvent delivery system, an automatic injector, a column thermostat, a DAD detector, and a HP Chemstation data acquisition system. Chromatograms of Naproxen enantiomers were recorded using the standard DAD detector. For other measurements, a HP 1037A refractive index (RF) detector connected to the data acquisition system through an Agilent 35900E Interface was used. The extra-column volumes in elution experiments were 0.029 and 0.168 ml, as measured from the autosampler to the DAD or RF detector cell, respectively. The extra-column volume in frontal analysis experiments was 0.621 ml, as measured from the pump to the DAD detector. All the retention data were corrected for these contributions.

3.2. Chemicals

The components of the mobile phases, HPLC grade water, methanol, and acetic acid were purchased from Fisher Scientific (Fair Lawn, NJ, USA). Deuterated methanol (99.8%) used for hold-up volume measurements was from Alfa Aesar (Ward Hill, MA, USA). (*S*)-Naproxen was from Cayman Chemicals and (*R*)-Naproxen from Sigma–Aldrich (St. Louis, MO, USA). Their purity was verified by HPLC. The content of the other enantiomer was found to be less than 0.2 and 0.5% for the (*S*)- and (*R*)-enantiomer, respectively.

3.3. Chromatographic column

A 250 mm×4.6 mm column packed with ~2.5 g of endcapped (*R,R*)-Whelk-O1 material, 10 μm particle size, 100 Å pore size, spherical silica was used. It was a gift of Regis Technologies (Morton Grove, IL, USA). The surface area of the silica was 200 m^2/g and its internal porosity 0.5 cm^3/g, as reported by the manufacturer. Before experiments, the column was flushed with 200 ml of isopropanol and 200 ml of methanol and then flushed with the mobile phase for no less than 1 h at a flow rate of 1 ml/min.

3.4. Procedures

3.4.1. Excess adsorption from binary mixtures methanol–water

The excess adsorption isotherms of methanol and water were determined by means of the minor perturbation method, as described in details in [16,31]. The measurements were carried out at 27 °C. The flow rate was kept at 1 ml/min. The measurement protocol was the same as in a previous publication [10]. The excess adsorption isotherms were calculated through the retention volumes of minor perturbations collected throughout the whole range of mobile phase compositions (from 0 to 100 vol.%), according to the following equation [16]:

$$\Gamma_i(c_{e,i}) = \frac{1}{V_a}\int_0^{c_{e,i}} (V_R(c_{e,i}) - V_0)\mathrm{d}c_{e,i} \tag{25}$$

where $V_R(c_{e,i})$ is the retention volume of the perturbation peak on the plateau of concentration $c_{e,i}$ of component *i*. The value of V_0 has the meaning of a thermodynamic hold-up volume [31] and is found from the normalization condition for Eq. (25):

$$V_0 = \int_0^{c_i^\star} V_{R,i}(c_i)\mathrm{d}c_i \tag{26}$$

where $c_i^\star$ is the molar concentration corresponding to the pure solvent *i*.

3.4.2. Measurement of the hold-up volume by the isotopic method

A value of the hold-up volume was derived from Eq. (26). Another value was evaluated by the isotopic method [32] based on the retention volume of an isotopically labeled solute in the same but nonlabeled solvent. Measurements were made at 27 °C, using pure methanol as the mobile phase and deuterated methanol as the tracer. The tracer concentration was 1 vol.%, the sample size 2 μl. The retention volume of the labeled methanol is equal to V_0 by definition [32].

3.4.3. Adsorption of Naproxen enantiomers

The adsorption of Naproxen was investigated by frontal analysis (FA) and by the inverse method. The mobile phase was a 0.01 M CH_3COOH solution in methanol–water (85/15, v/v) mixture. All experiments were made with this mobile phase composition.

3.4.3.1. Frontal analysis method. The FA method of determination of adsorption isotherms consists in measuring the amount of solute left in the column after this column has been flushed with a solution of concentration c^0 until adsorption equilibrium has been reached. This amount is given by integration of the transient curve ($c^0 - c(V)$), that is derived from the breakthrough curve $c(V)$, between V_0 and the volume for which $c(V) = c^0$. The breakthrough curves of the Naproxen enantiomers were generated using the multi-solvent delivery system of the chromatograph, by mixing streams of the pure mobile phase and a suitable analyte solution. Two series of FA runs were carried out, covering the high-concentration (1.6–8 g/l) and the low-concentration (0–0.8 g/l) ranges. Accordingly, two stock solutions of each enantiomer at 0.8 and 8 g/l were prepared in the mobile phase. The mixing ratio of the two streams was varied from 20:80 to 80:20 in steps of 20% for the low-concentration stock solution and from 20:80 to 90:10 in steps of 10% for the high-concentration stock solution. After each run, the column was washed with pure mobile phase.

The experiments were carried out at 27 °C. The breakthrough curves were recorded at a wavelength of 345 nm. The conversion of the detector signal to a concentration scale was performed with

the help of a nonlinear calibration curve [33] obtained during the same experiments. In the calculations, the V_0 value determined by the isotopic method as described in the previous section was used.

3.4.3.2. Determination of adsorption isotherms by the inverse method. The inverse method provides the numerical coefficients of a preselected isotherm model, through an optimization procedure that minimizes the distance between an experimental chromatogram and the profile calculated with a suitable model of chromatography [21]. The equilibrium-dispersive (ED) model of chromatography [21] was used in the present calculations. Numerical procedures are described in complete details elsewhere [10,34].

3.5. Study of mass transfer kinetics

The measurements of peak broadening were carried out at 27 °C, in the flow rate range 0.15–2.0 ml/min by injections of 2 μl samples of the racemic Naproxen. Each injection was repeated twice. The concentration of the sample was 0.4 g/l. In preliminary experiments, it was found that the retention time remains constant even after a fivefold decrease in the sample concentration. This proves that the measurements are carried out in the linear range of the adsorption isotherm, which is the mandatory condition for the determination of the pure kinetic broadening. Measurements at each flow rate studied were repeated without the column to evaluate the effect of extra-column dispersion. All results were corrected for that contribution.

Recorded chromatograms (wavelength 254 nm) were approximated by the exponentially modified Gaussian function [35] to eliminate the influence of signal noise on the results. It was those approximated profiles that were used to calculate the moments of peaks.

4. Results and discussion

4.1. Adsorption of methanol–water mixtures

Fig. 3 shows a plot of the reduced retention volume derived from the retention times of water and methanol perturbations versus the mobile phase composition. There is a good agreement between the two series of data. The V_0 value determined by Eq. (26) (2.890 ml) coincides very well with the value found by means of the isotopic method (2.888 ml).

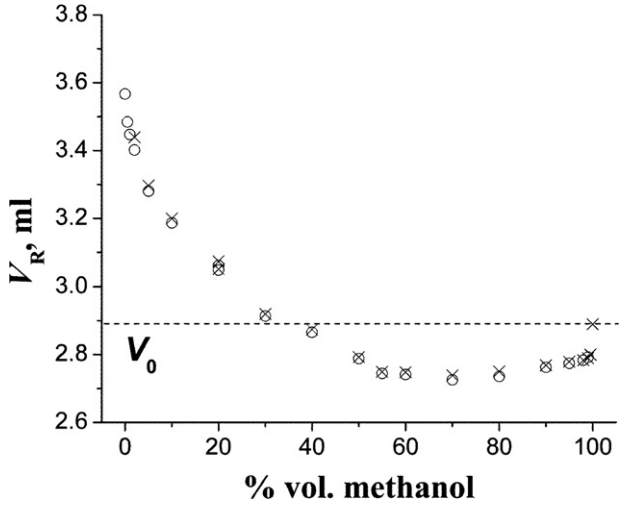

Fig. 3. Dependence of the retention of the minor perturbation peaks of methanol (circles) and water (crosses) from methanol–water solutions on the methanol volume fraction.

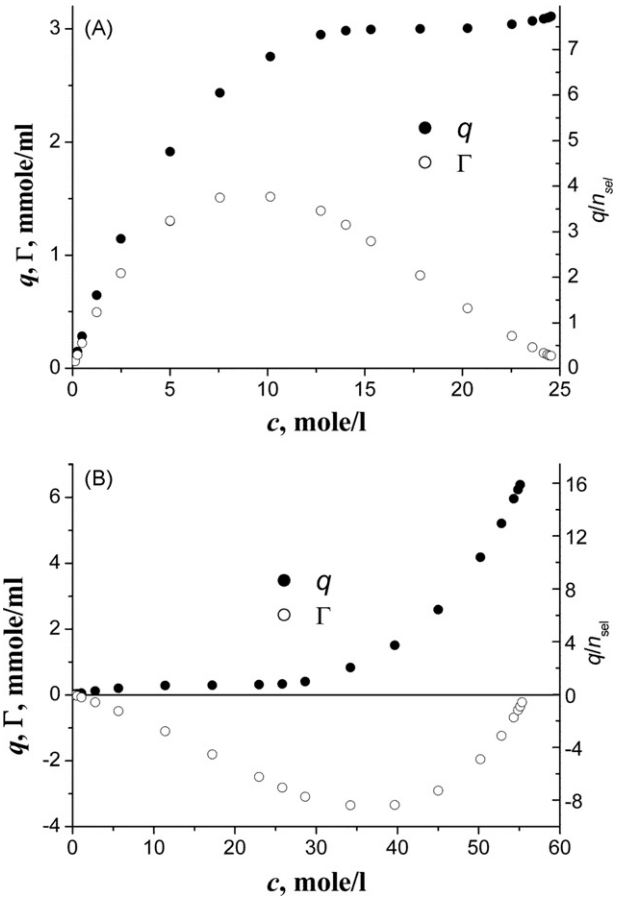

Fig. 4. Total and excess adsorption isotherms of methanol (A) and water (B) at 27 °C. The right ordinate axis shows the number of solvent molecules per chiral selector (n_{sel} is the concentration of chiral selectors).

The excess adsorption isotherms for methanol–water mixtures are given in Fig. 4, which shows that the adsorption of methanol is positive and that of water negative throughout the entire range of solution compositions. Thus, the grafted organic layer is relatively hydrophobic, expelling water in the presence of methanol, which can be accounted for by the influence of the large tetrahydrophenanthryl fragment of the chiral selector (see Fig. 2). The same conclusion was drawn in earlier work [10], where a sample of non-endcapped Whelk-O1 material was investigated. The excess adsorption isotherms had a similar shape, with only minor qualitative differences. This suggests that endcapping does not strongly affect the hydrophobicity of the stationary phase because of the shielding effect of bonded chiral selectors.

It must be noted that a negative excess adsorption does not mean complete exclusion of water from the adsorbed layer. It merely indicates a decrease of its concentration compared to that in the bulk phase. The isotherm of total adsorption (Fig. 4) evinces the presence of water in the stationary phase while there is water in the mobile phase. These isotherms were calculated using Eq. (2) with the δ value determined after ref. [16], based on an earlier work of Everett [17]. According to this method, δ is derived from the slope of the linear part of the excess adsorption isotherm of the preferentially adsorbed component. This gives a thickness of 3.1 Å for the adsorbed layer of methanol, which indicates a thin adsorbed layer, less than two van der Waals radii of a methanol molecule. A close value was reported for the adsorption of methanol from aqueous solutions on different reversed-phase adsorbents [16,36], for the non-endcapped CSP this value was found to be 2.1 Å [10]. Consid-

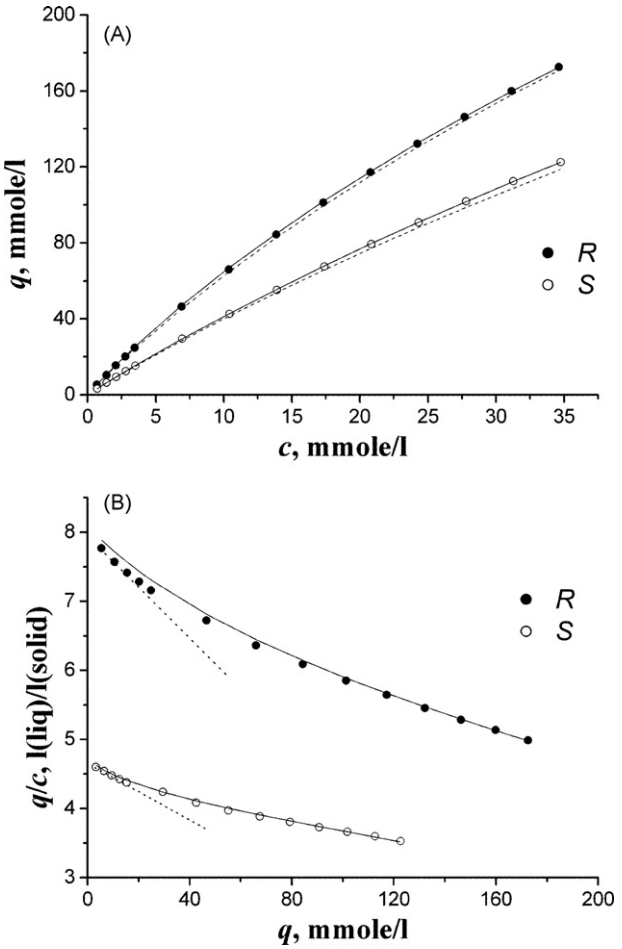

Fig. 5. Adsorption isotherms of the Naproxen enantiomers measured by the FA method (circles) and calculated by the inverse method (lines). Solid and dashed lines show the isotherms reconstructed based on the best fitting coefficients derived from the FA chromatograms (feed concentration 8 g/l) and from the elution chromatograms (sample concentration 8 g/l, sample volume 20 μl), respectively. The isotherms represented in the conventional (A) and Scatchard plot (B) coordinats. The dashed tangent lines in section (B) demonstrate the slopes of the Scatchard plots at a low-concentration part of an adsorption isotherm.

eration of the total adsorption isotherms suggests that complete filling of the adsorption layer by methanol (~ 7 molecules per a chiral selector) is achieved for a bulk phase composition of ~50% methanol (v/v).

4.2. Adsorption of Naproxen

Fig. 5 shows the adsorption isotherms of (*S*)- and (*R*)-Naproxen determined by the FA method in the conventional and the Scatchard coordinates. The Scatchard plots demonstrate a deviation from Langmuir isotherm behavior that is usually interpreted as demonstrating that the bi-Langmuir model accounts better for adsorption in enantioselective systems. However, the fitting of the adsorption data to Eq. (4) showed some discrepancy between the experimental data and the best fitted bi-Langmuir isotherm in the low-concentration region when the conditions in Eq. (5) were applied. This result was confirmed by the numerical calculation of the breakthrough profiles. When the profiles of both enantiomers were calculated simultaneously using the best isotherms fitted to the experimental data and applying Eq. (5), the profiles obtained exhibited moderate systematic deviations from the experimental records. The detailed description of the results of these calculations is omitted for the sake of brevity but it is worth to note here that the number of high-energy sites (~1 mmol/l) appeared to be much lower than that of low-energy sites (~600 mmol/l).

Careful consideration of the Scatchard plots (Fig. 5b) explains the failure of the simple bi-Langmuir model. The slopes of the plots for the (*S*)- and the (*R*)-enantiomers at the origin of coordinates differ. Near this origin, retention is determined by adsorption on the highest energy sites. Therefore, the difference in the slopes of the q/c *vs.* q plots shows that the high-energy sites exhibit enantioselectivity. However, the strongest sites, which are also the less abundant ones according to the bi-Langmuir analysis, must be associated with the nonselective residual silanol groups for the following reasons: (1) the relatively high selectivity of the Whelk-O1 column toward the Naproxen enantiomers ($\alpha = 1.74$ at 27 °C) suggests a rather low density of the nonselective sites, (2) bare silica is known to bear free silanol groups responsible for the strong retention of polar solutes but the density of these groups is small [37]; it is even smaller on bonded surfaces. The most likely explanation of this apparent contradiction is that some chiral selectors that interact with the more retained enantiomer ((*R*)-Naproxen) are close to some high-energy nonselective sites, making a small group of sites that are much stronger than the others. The coexistence of different groups of sites corresponding to the same chiral selector, is not uncommon in chiral systems involving low-molecular weight selectors. For instance, Lindner and coworkers [38,39] reported that in solutions there are several coexisting conformations of carbamoylated chincona alkaloids interacting differently with chiral molecules.

Consider the extension to the bi-Langmuir model according to the findings discussed earlier. Let b_{s1} and b_{s2} be the adsorption coefficients for those low- and high-energy enantioselective sites, respectively. If the total surface concentration of enantioselective sites is $q_s^\star$ and the concentration of the latter enantioselective sites $q_{s2}^\star$, the concentration of the sites of the first type is $(q_s^\star - q_{s2}^\star)$. From the above discussion it follows that $b_{s1,R} \neq b_{s2,R}$. At the same time, it is reasonable to accept $b_{s1,S} = b_{s2,S}$, which means that, for (*S*)-Naproxen, all the chiral sites are low-energy ones since, whatever physical factors may cause the differentiation of the enantioselective selectors in these two groups, these factors cannot affect significantly the strength of the sterically unfavorable interactions that take place with the less retained enantiomer because the latter cannot enter the chiral cleft.

The resulting adsorption isotherms are

For (*S*)-Naproxen:

$$q = \frac{q_{ns}^\star b_{ns} c}{1 + b_{ns} c} + \frac{q_s^\star (b_{s1,S}) c}{1 + (b_{s1,S}) c} \tag{27}$$

for (*R*)-Naproxen:

$$q = \frac{q_{ns}^\star b_{ns} c}{1 + b_{ns} c} + \frac{(q_s^\star - q_{s2}^\star)(b_{s1,R}) c}{1 + (b_{s1,R}) c} + \frac{q_{s2}^\star (b_{s2,R}) c}{1 + (b_{s2,R}) c} \tag{28}$$

The adsorption equilibrium constants at infinite dilution for these two equations are respectively:

$$K_{H,S} = h_{s1,S} + h_{ns} = q_s^\star b_{s1,S} + q_{ns}^\star b_{ns} \tag{29}$$

and

$$K_{H,R} = h_{s1,R} + h_{s2,R} + h_{ns} = (q_s^\star - q_{s2}^\star) b_{s1,R} + q_{s2}^\star b_{s2,R} + q_{ns}^\star b_{ns} \tag{30}$$

where h_i ($i = s1, s2, ns$) stands for the contributions of the i type of adsorption sites to the total retention.

This model gives excellent agreement between the experimental and calculated isotherms (Fig. 5) and band profiles (Fig. 6). Table 1 lists the parameters of the model used in the calculations of the isotherms and chromatograms presented in these figures. Those parameters were found using data provided by the inverse method applied to the desorption branches of the frontal chromatograms of the two enantiomers at the highest mobile phase

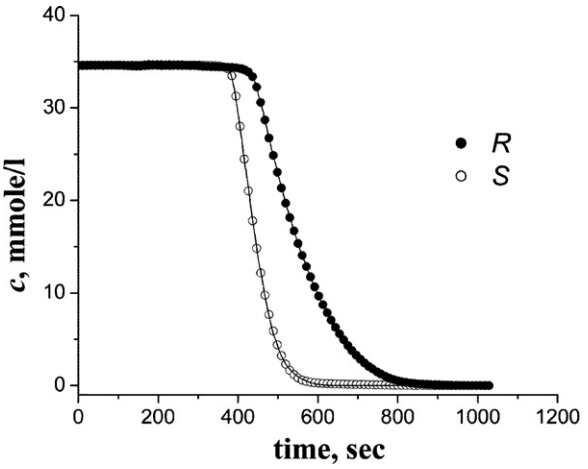

Fig. 6. Comparison of desorption profiles of the Naproxen enantiomers measured experimentally (circles) and calculated by means of the inverse method. Feed concentration was 8 g/l, flow rate 1 ml/min.

concentration studied. The total saturation capacity of the enantioselective sites is approximately equal to the value of the Whelk-O1 chiral selectors concentration (422 mmol/l) found in the literature [9]. This substantiates the physical soundness of the best fit model parameters. The concentration of the nonselective sites accounts for only 0.36% of the total saturation capacity. Combined with a high value of the coefficient b_{ns}, this is consistent with the attribution of the nonchiral adsorption sites to the residual silanols of the silica support.

The model proposed neglects the dissociation of Naproxen in the mobile phase. Estimates of the dissociation degree of this acid in the methanol–water mixture of interest (see Ref. [40]) give 0.2 and 0.3% for the highest and the lowest solute concentration studied. The fraction of anions in the adsorption layer consisting mostly of pure methanol must be still smaller. This justifies omitting consideration of the dissociation effects.

The negligible dissociation of the analyte in the mobile phase distinguishes the adsorption system studied here from the one explored in an earlier work [10], in which, due to the use of buffered eluents (acetic buffer), the mobile phase pH was kept at 5.4–5.9, setting the dissociation degree to ca. 20%. This resulted in an adsorption behavior somewhat different from that observed in the present work. So, the equilibrium model needed for the preceding system did not require the assumption of two groups of chiral selectors adsorbing differently to explain the band profiles of the more retained enantiomer. Besides, the front dispersion of the band profile of the less retained enantiomer reported in [10] for a methanol concentration of 80% (v/v) was not observed here, although the mobile phase methanol concentration was higher, 85%. Even when the methanol concentration (in an unbuffered mobile phase) was

Table 1
Best fit parameters of the adsorption isotherms found by the FA (in italics) and elution method [a].

Parameter	Temperature, °C				
	22.0	*27.0*	27.0	34.7	40.0
q_s, mmol/l	649	*677*	656	680	862
$b_{s1,S}$, l/mmol	0.0074	*0.0062*	0.0062	0.0052	0.0034
$b_{s1,R}$, l/mmol	0.0111	*0.0090*	0.0098	0.0073	0.0049
q_{s2}, mmol/l	11.0	*18.3*	3.5	9.4	5.1
$b_{s2,R}$, l/mmol	0.207	*0.091*	0.316	0.119	0.143
q_{ns}, mmol/l	2.41	*2.47*	2.21	0.69	2.24
b_{ns}, l/mmol	0.289	*0.203*	0.242	0.450	0.182

[a] The relative confidence intervals for coefficients q_s, $b_{s1,S}$, $b_{s1,R}$, q_{s2}, $b_{s2,R}$, q_{ns}, and b_{ns} were less than 4.6, 5, 9, 5, 6, and 5%, respectively (confidence probability 95%).

Table 2
The effect of temperature on the Henry coefficient and selectivity of (*R*, *R*)-Whelk-O1.

T, °C	(*S*)-Naproxen			(*R*)-Naproxen				α [a]
	h_{s1}	h_{ns}	K_H	h_{s1}	h_{s2}	h_{ns}	K_H	
22.0	4.82	0.70	5.51	7.11	2.28	0.70	10.08	1.83
27.0	4.08	0.53	4.62	6.41	1.11	0.53	8.05	1.74
34.7	3.53	0.31	3.84	4.86	1.12	0.31	6.28	1.64
40.0	2.96	0.41	3.36	4.22	0.73	0.41	5.36	1.60

[a] $\alpha = K_H(R)/K_H(S)$.

90%, the shape of the first eluted peak was Langmuirian (data not shown). On the other hand, the underlying properties of the adsorption systems of consideration are similar. The coexistence of the enantioselective and nonselective adsorption sites with a major predominance of the former ones was convincingly suggested in both studies. The values of the saturation capacities for both columns are in good agreement, considering that these were determined for nonidentical CSPs (endcapped and non-endcapped) with rather different mobile phases.

4.2.1. The effect of temperature

The temperature influence on adsorption gives valuable information on the thermodynamics of adsorption, therefore on the nature of the processes involved. Due to the high cost of pure enantiomers, the measurement of adsorption isotherms by the FA method at different temperatures was not affordable. Measurements made with the inverse method require much lower amounts of reagents. They were carried out at 22, 27, 34.7, and 40 °C, using a 8 g/l solution of each enantiomer. The sample volume injected was 20 μl. The region of equilibrium concentrations that can be explored with this method is much smaller than with the FA mode. It is not rare that the information derived from peak profiles is somewhat distorted. This mainly concerns the characteristics of the most abundant type of adsorption sites, which definitely cannot be saturated under such conditions. Therefore, some validation of the results of this method of measurements of adsorption isotherms is desirable. Fig. 5 compares the isotherms obtained by the two methods considered at 27 °C. Fig. 5a shows the excellent agreement between the (*R*)-Naproxen isotherm plot drawn using the best fit coefficients found with the elution and the FA methods. The agreement is not as good for (*S*)-Naproxen at high concentrations, but it is very good at low concentrations, particularly in the range covered in the elution experiments. Note also that the values of the best fit parameters found by both methods are in good agreement except for the $q_{s2,R}$ and $b_{s2,R}$ coefficients that are of the same order of magnitude (Table 1).

The elution profiles calculated by the inverse method and those recorded coincide completely for both enantiomers, at all the temperatures studied (data not shown). The best fitting parameters of the adsorption model at different temperatures are listed in Table 1, the respective values of the Henry coefficient are listed in Table 2. Considering these data the following conclusions can be drawn:

(1) A major fraction of the sites of selective interactions are low-energy sites. These sites do determine the retention because their density is a thousand times larger than that of the nonselective adsorption sites. Their contribution to retention at infinite dilution amounts to about 12 and 7% for (*S*)- and (*R*)-enantiomers, respectively, and does not depend on the temperature within the limits of experimental error.
(2) Both the Henry coefficients and the contributions to these coefficients of the different adsorption mechanisms (*h*-terms) decrease with increasing temperature, even though some adsorption coefficients do not show a clear temperature

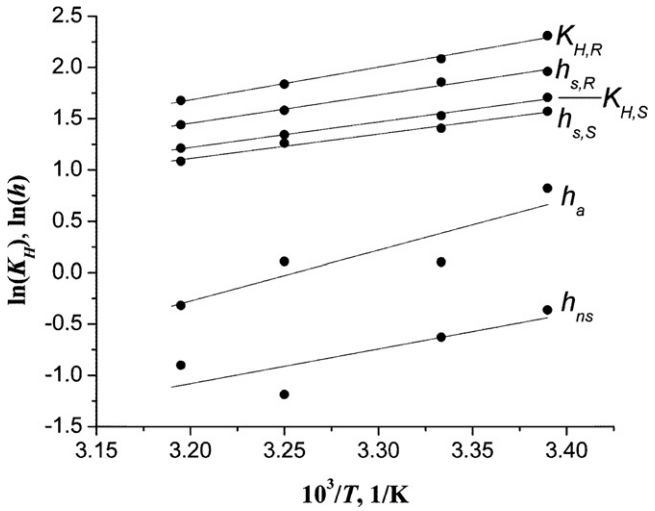

Fig. 7. Van't Hoff plots of the Henry coefficients and h-terms (see notices on the right side of the graph). Circles represent experimental data, lines are results of linear regression.

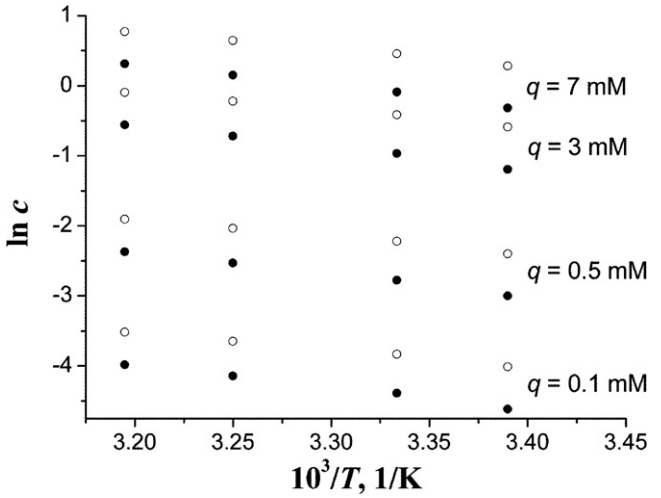

Fig. 8. Adsorption isosters of (*R*)—(filled circles) and (*S*)—Naproxen (open circles) at different values of adsorbed amount (shown on the right side of the graph). Dimension of concentration is mmol/l.

dependence, like b_{ns} and $b_{s2,R}$. The latter is most likely due to a mutual statistical correlation of adjustable parameters in the products ($q_{ns}b_{ns}$) and ($q_{s2,R}b_{s2,R}$).

(3) The concentration of the selective sites increases with increasing temperature. The monotonous character of this trend suggests that it has a physical, not a statistical origin. There are reports in the literature of increasing [41] and decreasing [42] trends of the saturation capacity of Pirkle-type CSPs with increasing temperature. That it increases in this case may indicate a weakening of the shielding effect of the adsorption of the mobile phase components with increasing temperature.

Fig. 7 shows the temperature dependencies of the Henry coefficients and the h-terms in the van't Hoff coordinates. The corresponding enthalpy characteristics of adsorption are listed in Table 3. The total adsorption enthalpy (ΔH) is somewhat larger than the adsorption enthalpy on the low-energy selective sites (ΔH_{s1}), revealing a minor contribution of high-energy adsorption. This effect is more visible for the (*R*)-enantiomer because of the strongly exothermal adsorption on high-energy enantioselective sites. The absolute values of $\Delta H_{s1,S}$ and $\Delta H_{s1,R}$ are usual for liquid/solid adsorption with a specific interaction (e.g., $\pi-\pi$ stacking, dipole–dipole interactions, and hydrogen bonding). The enthalpy $\Delta H_{s2,R}$ is remarkably high, suggesting a certain contribution of Coulomb interactions. Although this quantity was not estimated with precision, it is statistically significant at the $P = 0.9$ confidence level.

The data in Table 3 characterize the linear part of an adsorption isotherm. The influence of nonlinear behavior on adsorption thermodynamics could be described by the dependence of the isosteric enthalpy of adsorption (ΔH_{st}) on the adsorbed amount. The quantity of ΔH_{st} is defined as

$$\Delta H_{st} = -RT^2\left(\frac{\partial \ln c}{\partial T}\right)_q \tag{31}$$

Some examples of the adsorption isosters are shown in logarithmic coordinates in Fig. 8. A slight nonlinear behavior is peculiar to these plots. Nonetheless, the degree of nonlinearity is not high (the regression coefficient is $r^2 > 0.99$), which justifies an estimation of ΔH_{st} via the slope of the corresponding logarithmic isosters. Fig. 9 exhibits plots of $\Delta H_{st}(q)$ for the Naproxen enantiomers. Their values are close to the enthalpies found for the Henry coefficients. The shape of the plots of $(-\Delta H_{st})$ *vs.* q is different for the (*S*)- and the (*R*)-Naproxen. The curve decreases monotonically for the more retained enantiomer and has a feeble maximum for the less retained enantiomer. In the latter case, the amplitude of the maximum is much less than the range of variation of the enthalpy in the former case. A similar situation was observed for the adsorption of the enantiomers of 3-chloro-1-phenylpropanol on a Pirkle-type CSP (silica bonded quinidine carbamate) [42]. It can be explained by the fact that a sterically favorable interaction is more sensitive to secondary factors (minor changes in conformation of a chiral selector, in the influence of neighboring surface groups and so on) than a sterically unfavorable one. As a result, the adsorption

Table 3
Enthalpy characteristics of adsorption (in kJ/mol) and their standard deviations (in brackets).

	Parameter [a]	(*S*)-Naproxen	(*R*)-Naproxen
$-\Delta H$	K_H	20.7 (1.1)	26.6 (1.3)
$-\Delta H_{s1}$	h_{s1}	19.8 (1.7)	23.0 (1.6)
$-\Delta H_{s2}$	h_{s2}		41 (14)
$-\Delta H_{ns}$	h_{ns}	28 (14)	

[a] Equilibrium coefficient used to find a respective enthalpy quantity.

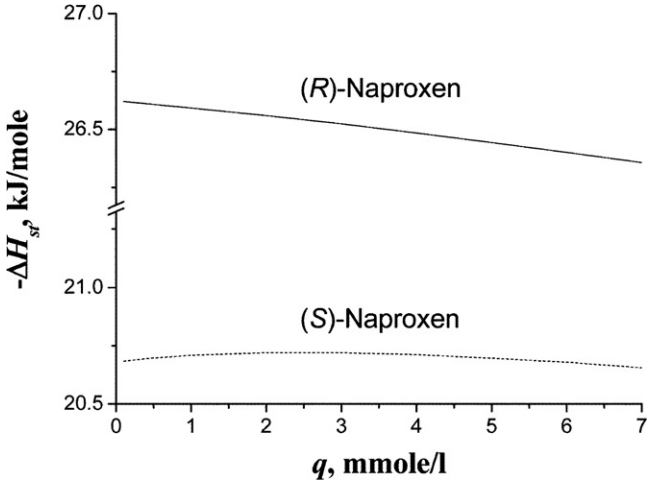

Fig. 9. Dependence of the isosteric enthalpy of adsorption on adsorbed amount.

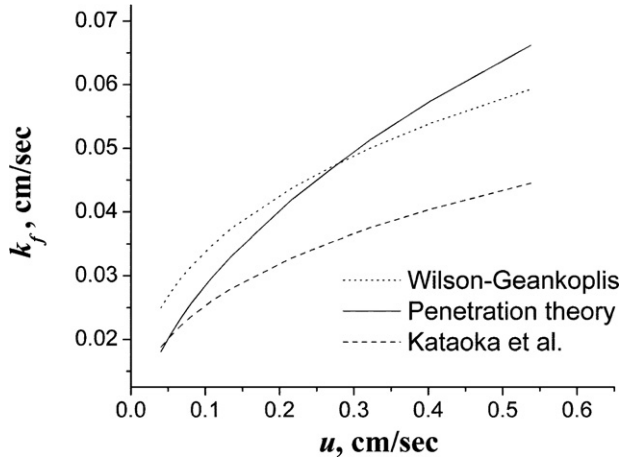

Fig. 10. Dependence of the external mass transfer coefficient on the interstitial flow velocity estimated by different methods.

energy distribution of the enantioselective sites is wider for the stronger retained enantiomer. Consequently, in this case, differential adsorption heat subsides faster as the coverage of the chiral selectors increases.

4.3. Mass transfer kinetics

In the theoretical section, it was shown that chromatographic measurements give only a lumped mass transfer coefficient, summarizing the contributions from the external and internal diffusion and from the adsorption kinetics. The determination of the contributions from diffusion processes relies on extra-chromatographic relationships. Then part of adsorption kinetics can be derived, based on a difference between the total resistance to mass transfer and the diffusion contribution. The evaluation of dynamic coefficients through empirical correlations is associated with some degree of uncertainty. Estimates of k_f according to the different approaches shown in Fig. 10 display a discrepancy of about 30% between the Wilson-Geankoplis and the Kataoka lines. The coefficient found by the penetration theory (Eq. (20)) varies between these two lines when the flow velocity increases. Miyabe et al. [43] have recently investigated the problem of assessment of the external mass transfer in HPLC. They concluded that the relative precision of k_f is approximately 20%. Another conclusion that can be drawn from this work is that all the available correlations give estimates of k_f, which are within the same confidence interval as the experimental values, therefore no particular correlation should be preferred. In this work, the Wilson-Geankoplis equation was chosen for no particular reason.

The evaluation of the internal diffusion term is the subject of some concern. First, it includes the molecular diffusivity calculated through the Wilke-Chang equation, whose error was reported to be of 10% [23]. Second, the accepted definition of D_p relies on a model of uniform three-dimensional network of channels [29], which is definitely a very simplified representation of the pore structure of stationary phases. This short discussion shows that the best that one can expect from mass transfer kinetics calculations is only an estimate of the order of magnitude of the mass transfer parameters. In the case of chiral adsorption, the situation is more favorable. A difference in the adsorption kinetics of enantiomers results only from some difference in the adsorption equilibrium coefficients and in adsorption rate constants. Therefore information obtained by comparing the peak broadening of enantiomers is free from uncertainties resulting from extra-chromatographic estimates of the external and intraparticle diffusion.

Table 4
Constants used for dynamic calculations.

Parameter	Value	Source
ϵ_e	0.37	[a]
ϵ_i	0.52	[b]
D_m, cm^2/s	0.64×10^{-5}	Eq. (17)
D_p, cm^2/s	7.73×10^{-7}	Eq. (21)

[a] Theoretical value based on the model of random packing of spheres [48]. This value is within a range 0.35–0.40 recommended by Ruthven [44] and frequently found in chromatographic studies.
[b] Calculated based on the given value of ϵ_e and on the value of V_0 found experimentally.

One more issue to mention before proceeding to a discussion of the body of experimental results is that k_f in Eq. (9) is assumed to be constant whereas it is a function of the flow rate (Fig. 10). Frequently an averaged k_f is used in the calculations. An alternate approach consists in subtraction the external mass transfer term from the HETP using the following analogs of the van Deemter and Giddings equations:

$$H' = H - H_{ext} = A + \frac{B}{u} + C'u \tag{32}$$

$$H' = H - H_{ext} = \frac{1}{1/a + 1/(bu)} + \frac{B}{u} + C'u \tag{33}$$

$$H_{ext} = 2\left(\frac{k_1}{1+k_1}\right)^2 \frac{d_p u}{6F_e k_f(u)} \tag{34}$$

where the constant C' includes only intraparticle diffusion and adsorption kinetics terms:

$$C' = f_1 \left[\frac{d_p^2}{60F_e D_p} + \left(\frac{k_p}{1+k_p}\right)^2 \frac{1}{F_e k_{ads}}\right] \tag{35}$$

with

$$f_1 = 2\left(\frac{k_1}{1+k_1}\right)^2 \tag{36}$$

In theory, the latter method is more correct. Of course, its validity depends on how accurate the estimate of k_f is.

Both approaches were tested. The results obtained were qualitatively the same. In quantitative terms the discrepancy between the coefficients was less than 10–15%. Considering such a small difference and for the sake of brevity, only data involving the use of Eqs. (32) and (33) are discussed. A summary of the bed characteristics and the diffusion coefficients used in the calculations is given in Table 4.

4.3.1. HETP equation

Fig. 11A compares the HETP data for both enantiomers. All the data belong to the ascending branch of the $H(u)$ function. Hence the influence of molecular diffusion on band broadening within the velocity range investigated is negligible, which allows a simplification of the van Deemter and Giddings equations by assuming $B = 0$. Another important observation consists in the expected fact that the plots coincide in the low velocity region, where the influence of enantiospecific kinetic broadening is small but diverge in the high velocity region, where the kinetic broadening plays a considerable role. Thus, the use of the same adjustable parameters A and a, b for both enantiomers is experimentally justified. The results of the nonlinear regression analysis of the experimental data with Eqs. (32) and (33) (Fig. 11B) reveal a better agreement of the Giddings theory with experimental data. The best fitting parameters of Eq. (33) are $a = 0.00267$ cm, $b = 0.153$ s, $C'(S) = 0.0138$ s, and $C'(R) = 0.0148$ s.

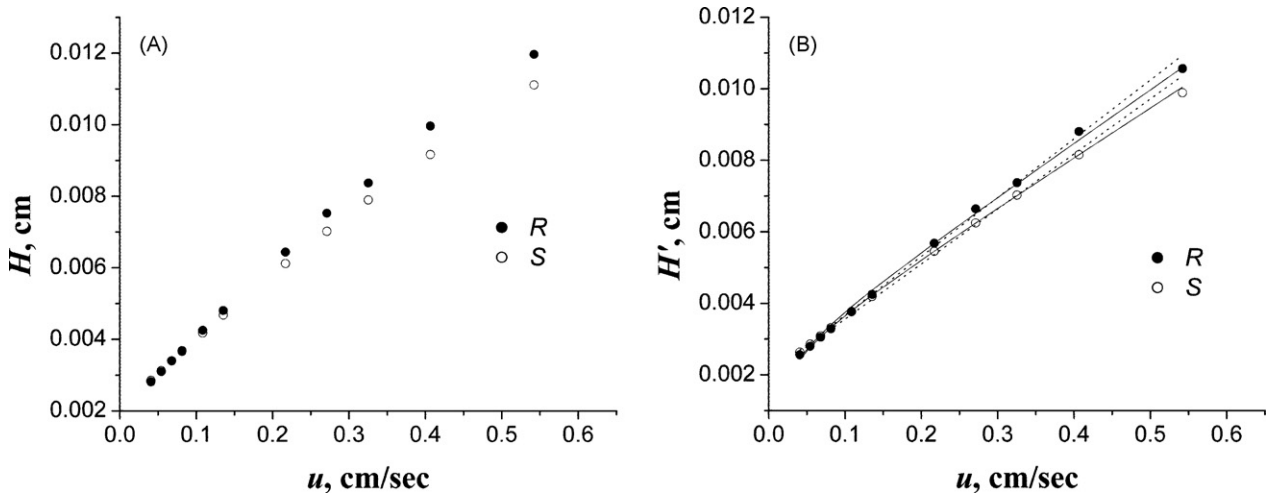

Fig. 11. Plots of HETP (A) and HETP corrected for the external mass transfer contribution (B) as a function of the interstitial flow velocity.

It is interesting to evaluate the contributions to band dispersion of the different factors in the HETP equation. Those from axial dispersion, the external and intraparticle mass transfer, $H_{ax} = H_{cpl}$ (See Eq. (14)), H_{ext}, and $H_{int} = C'u$, respectively, are shown in Fig. 12. For the sake of clarity, only data for the (*R*)-enantiomer are given. The graph shows that the external mass transfer has a minor contribution to band dispersion. The contribution of axial dispersion plays a major role at low flow velocities, but less above 0.15 cm/s. At higher u the importance of the H_{int} term, that depends linearly on the flow velocity, progressively increases, exceeding the influence of axial dispersion. Some factors of chromatographic band dispersion are considered in more details below.

4.3.1.1. Axial dispersion. Fig. 13 compares the plots of the axial dispersion coefficients calculated by different methods as a function of the interstitial velocity. The D_{ax} functionalities were calculated using Gunn method and through the Giddings equation as $D_{ax}(u) = (u/2)(1/a + 1/(bu))^{-1}$. The figure also shows a plot of the product $d_p u$ that is an estimate of the axial dispersion, according to van Deemter, when molecular diffusivity is assumed to be negligible and the parameter $\gamma_2 \sim 1$. In general, the van Deemter and Gunn correlations yield close results. Thus the Gunn correlation that was derived from the stochastic model, in fact, predicts that axial band broadening is equivalent to the dispersive effect of eddy diffusion in packed beds. The apparent axial dispersion found from Eq. (33) is noticeably larger. It is almost a linear function of u and formally corresponds to a γ_2 value of 1.3. According to Ruthven [44] and Tsotsas and Schlünder [45] a typical value for this constant is 0.5. Consequently, the loss of efficiency due to axial dispersion for the current column would be 2.6 times larger than for a conventional well-packed bed.

4.3.1.2. Adsorption kinetics. The C' coefficient of the Giddings Eq. (33) accounts for the resistance to mass transfer due to intraparticle diffusion and to the kinetics of adsorption–desorption. The reciprocal value of C' corrected for the factor f_1 has the unit of a lumped mass transfer coefficient. The values of the retention factor at infinite dilution needed to compute k_1 were found from the same chromatograms that were used for the measurements of the HETP. These values averaged over all the flow rates examined were used in the calculations. The results in a form of Henry coefficients are presented in Table 5. The difference between the mass transfer parameters of the enantiomers derived from C' is small, 6.6%, but yet it is meaningful since the error made on the retention factor (0.7%) can account for only 0.2% of this difference. It must also be mentioned that although C' is a kinetic parameter, it depends

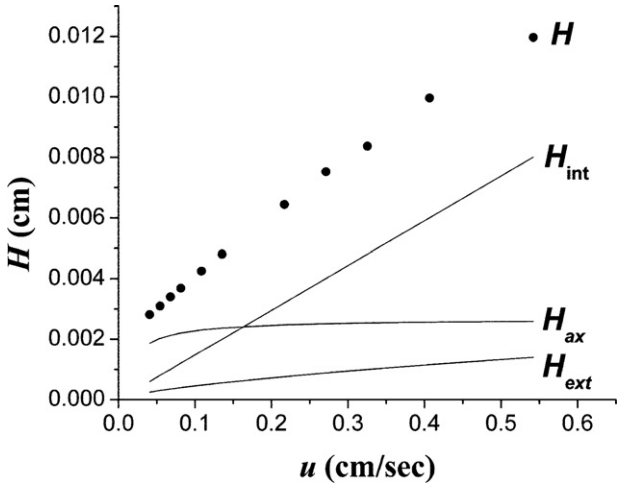

Fig. 12. HETP of (*R*)-Naproxen and its contributions as a function of the interstitial flow velocity. Symbols represent experimentally measured HETP values (H), lines represent the contributions in the HETP value from axial dispersion (H_{ax}), the external mass transfer (H_{ext}), and the intraparticle mass transfer (H_{int}).

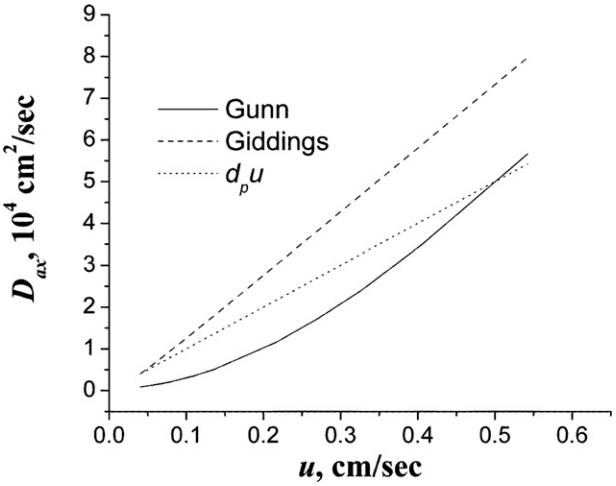

Fig. 13. Dependence of the axial dispersion coefficient on the interstitial flow velocity estimated by different methods.

Table 5
Comparison of equilibrium and adsorption kinetics characteristics of the Naproxen enantiomers.

Parameter	(*S*)-Naproxen	(*R*)-Naproxen
K_H	4.72 ± 0.03	8.27 ± 0.07
f_1	1.367	1.566
f_1/C', 1/s	99.4	106.0
C'/f_1, s	0.0101	0.0094
$d_p^2/(60F_eD_p)$, s	0.0127	

on the adsorption equilibrium constant through the f_1 factor. It is the thermodynamic effect that determines a poorer efficiency for (*R*)-Naproxen because, according to the net kinetic characteristics (C'/f_1; see Table 5), the peak broadening for this enantiomer should be smaller than that of the less retained enantiomer, however, it is larger due to a higher value of f_1.

The coefficient C' includes two terms, one for intraparticle diffusion, the other for adsorption. The first contribution can be estimated based on Eq. (21). The corresponding figures in Table 5 show that the diffusion term exceeds C'/f_1, which is meaningless. This contradiction could be explained by the influence of surface diffusion [46]. Indeed, if the effective intraparticle diffusion coefficient, D_{eff}, including surface diffusion (Eq. (37)) is used instead of pore diffusivity, one can adjust the intraparticle diffusion term to the C' value by fitting of D_s:

$$D_{eff} = D_p + (1 - \epsilon_i)K_H D_s \quad (37)$$

That the expression of the surface diffusion term includes K_H explains the enantioselective character of the (f_1/C') ratio. That the adsorption rate contribution is ignored in this case is arguable. Unfortunately, chromatographic experiments cannot separate the effects of surface diffusion and of the adsorption process proper. In the same time, it is clear that the difference observed between the coefficients $C'(S)$ and $C'(R)$ can only be ascribed to the different kinetics of interaction of the two enantiomers with the chiral selectors, whichever of the two mechanisms benefits from this interaction, the transfer of a solute molecule to an adsorption site from a neighboring adsorption site (surface diffusion) or the capture of a solute molecule by an adsorption site from the liquid phase (adsorption kinetics). The difference observed in the kinetic behavior of the enantiomers is small in spite of a considerable difference between the adsorption equilibrium coefficients. This is understandable because the stationary phases used in liquid chromatography are designed for promoting rather weak adsorption and allow short analysis times. This implies fast adsorption and desorption rates, which results in moderate or low peak broadening compared with other mass transfer processes. Therefore in the C' constant, the effect of enantioselective mass transfer (either originated from surface diffusion or from adsorption kinetics) is masked by the non-enantioselective pore diffusion, the influence of which is always significant.

5. Conclusion

The adsorption of Naproxen enantiomers on the (*R*, *R*)-Whelk-O1 CSP from a methanol–water solution modified with the addition of acetic acid was studied in detail. The CSP was found to exhibit hydrophobic properties. For a 85:15 (v/v) methanol–water mobile phase, the water content in the adsorbed layer is minor, 7.3 mol.%, that is equivalent to ~0.6 water molecules per chiral selector. The adsorption behavior of Naproxen is well accounted for by a model of a CSP surface covered with two different types of adsorption sites, enantioselective and nonselective. The adsorption data show that there are two sorts of enantioselective sites, sparse strong adsorption sites that preferentially retain the (*R*)-enantiomer and account for 1 to 2% of the total enantioselective sites and numerous weak enantioselective adsorption sites. The total concentration of the enantioselective sites (~670 mmol/l) is roughly close to the surface density of chiral selectors. It is three orders of magnitude higher than the concentration of the nonselective sites (0.2–0.3 mmol/l) that have a high adsorption affinity toward the analyte and are associated with the residual free silanols of silica surface. Due to their much higher concentration, the enantioselective sites make a major contribution to the retention of Naproxen and to the total thermal effect of adsorption.

A van't Hoff analysis undertaken separately for each term of the adsorption isotherm showed that the thermodynamics of adsorption on the low-energy enantioselective sites is typical of liquid/solid adsorption involving weak specific interactions like hydrogen bonding, $\pi - \pi$, and dipole–dipole interactions. In contrast, the adsorption enthalpy on the nonselective sites is characterized by a somewhat higher absolute value. The enthalpy of adsorption on the high-energy enantioselective sites is typical of ion–ion interactions in solutions suggesting the formation of a strong adsorbed complex with intense polarization of the select and inside the chiral cleft of the selector moiety.

Column dynamics follows Giddings HETP equation, suggesting an influence of the coupling effect on eddy diffusion. The extent of the axial dispersion term is slightly larger than for conventional packed columns without resulting in a noticeable decrease of the efficiency. As the flow velocity increases, the $H(u)$ curves of the two enantiomers, which coincide at low concentrations, diverge. Although this could result from the different retention, a detailed analysis reveals an effect of kinetic nature. The difference between the kinetic parameters of the enantiomers is small and the study of the kinetics of interactions of the two enantiomers with the chiral selectors shows it to be hindered by the masking influence of intraparticle diffusion, which is an achiral process. This influence could be avoided by using non-porous particles of stationary phases like Kovasil [47] that would be promising solids to study the kinetics of enantioselective adsorption. To the best of our knowledge, no investigations of this field have been attempted yet, in spite of its potential interest.

Acknowledgments

This work was supported by grant CHE-06-08659 of the National Science Foundation and by the cooperative agreement between the University of Tennessee and the Oak Ridge National Laboratory. The authors highly appreciate the generous gift of a column by Ted Szczerba (Regis Technologies, Morton Grove, IL, USA).

References

[1] W.H. Pirkle, Ch.J. Welch, J. Liq. Chromatogr. 15 (1992) 1947–1955.
[2] Ch.J. Welch, J. Chromatogr. A 666 (1994) 3–26.
[3] W.H. Pirkle, Ch.J. Welch, J. Chromatogr. A 683 (1994) 347–353.
[4] W.H. Pirkle, Ch.J. Welch, Tetrahedron: Asym. 5 (1994) 777–780.
[5] Ch. Wolf, W.H. Pirkle, Tetrahedron 8 (2002) 3597–3603.
[6] M.E. Koscho, P.L. Spence, W.H. Pirkle, Tetrahedron: Asym. 16 (2005) 3147–3153.
[7] G.E. Job, A. Shvets, W.H. Pirkle, S. Kuwahara, M. Kosaka, Y. Kasai, H. Taji, K. Fujita, M. Watanabe, N. Harada, J. Chromatogr. A 1055 (2004) 41–53.
[8] A. Del Rio, J.M. Hayes, M. Stein, P. Piras, C. Roussel, Chirality 16 (2004) S1.
[9] C.F. Zhao, S. Diemert, N.M. Cann, J. Chromatogr. A 1216 (2009) 5968–5978.
[10] L. Asnin, F. Gritti, K. Kaczmarski, G. Guiochon, J. Chromatogr. A 1217 (2010) 264–275.
[11] Ch.J. Welch, T. Szczerba, S. Perrin, J. Chromatogr. A 758 (1997) 93–98.
[12] J. Zheng, S.A. Shamsi, J. Chromatogr. A 1005 (2003) 177–187.
[13] A.C. Sehgal, R.M. Kelly, Biotechnol. Prog. 19 (2003) 1410–1416.
[14] J. Dungelova, J. Lehotay, J. Cizmarik, D.W. Armstrong, J. Liq. Chromatogr. 26 (2003) 2331–2350.
[15] J. Dungelova, J. Lehotay, J. Krupčik, J. Cižmarik, D.W. Armstrong, J. Sep. Sci. 27 (2004) 983–990.
[16] Y.V. Kazakevich, R. LoBrutto, F. Chan, T. Patel, J. Chromatogr. A 913 (2001) 75–78.
[17] D.H. Everett, J. Chem. Soc., Faraday Trans. I 60 (1964) 1803–1813.
[18] E.A. Guggenheim, Thermodynamics, North-Holland, Amsterdam, 1967, 46.
[19] T. Fornstedt, P. Sajonz, G. Guiochon, Chirality 10 (1998) 375–381.

[20] L. Ravald, T. Fornstedt, J. Chromatogr. A 908 (2001) 111–130.
[21] G. Guiochon, A. Felinger, A.M. Katti, S.G. Shirazi, Fundamentals of Preparative and Nonlinear Chromatography, second ed., Academic Press, Boston, MA, 2006.
[22] J. Giddings, Dynamics of Chromatography. Principles and Theory, Marcel-Dekker, New York, 1965.
[23] B. Poling, J. Prausnitz, J. O'Connell, The Properties of Gases and Liquids, fifth ed., McGraw-Hill, New York, 2001.
[24] E. Wilson, C. Geankoplis, Ind. Eng. Chem. Res. Fundam. 5 (1966) 9–14.
[25] R.B. Bird, W.E. Stewart, E.N. Lightfoot, Transport Phenomena, Wiley, New York, 1962.
[26] D.D. Frey, E. Schweinheim, C. Horváth, Biotechnol. Prog. 9 (1993) 273–284.
[27] R. Sharma, D. Cresswellt, E. Newson, Ind. Eng. Chem. Res. 30 (1991) 1428.
[28] M. Barrande, R. Bouchet, R. Denoyel, Anal. Chem. 79 (2007) 9115.
[29] J.S. Mackie, P. Meares, Proc. Roy. Soc. (London) A232 (1955) 498–509.
[30] D. Gunn, Chem. Eng. Sci. 42 (1987) 363–373.
[31] Y.V. Kazakevich, H.M. McNair, J. Chromatogr. Sci. 31 (1993) 317–322.
[32] J.H. Knox, R. Kaliszan, J. Chromatogr. 349 (1985) 211–234.
[33] L. Asnin, G. Guiochon, J. Chromatogr. A 1089 (2005) 101–104.
[34] A. Felinger, A. Cavazzini, G. Guiochon, J. Chromatogr. A 986 (2003) 207–225.
[35] D. Hanggi, P.W. Carr, Anal. Chem. 57 (1985) 2394–2395.
[36] F. Gritti, G. Guiochon, Anal. Chem. 77 (2005) 4257–4272.
[37] J. Navrocki, J. Chromatogr. A 779 (1997) 29–71.
[38] N.M. Maier, S. Schetzick, G. Lombardo, M. Feliz, K. Rissanen, W. Lindner, K.B. Lipkowitz, J. Am. Chem. Soc. 124 (2002) 8611–8629.
[39] C. Czerwenka, M.M. Zhang, H. Kählig, N.M. Maier, K.B. Lipkowitz, W. Lindner, J. Org. Chem. 68 (2003) 8315–8327.
[40] F. Oumada, C. Ràfols, M. Rosés, E. Bosch, J. Pharm. Sci. 91 (2002) 991–999.
[41] G. Götmar, L. Asnin, G. Guiochon, J. Chromatogr. A 1059 (2004) 43–52.
[42] L.A.K. Kaczmarski, A. Felinger, F. Gritti, G. Guiochon, J. Chromatogr. A 1101 (2006) 158–170.
[43] K. Miyabe, M. Ando, N. Ando, G. Guiochon, J. Chromatogr. A 1210 (2008) 60–67.
[44] D. Ruthven, Principles of Adsorption and Adsorption Processes, Wiley-Interscience, New York, 1984.
[45] E. Tsotsas, E.U. Schlünder, Chem. Eng. Process. 24 (1988) 15–31.
[46] K. Miyabe, G. Guiochon, Adv. Chromatogr. 40 (2000) 1–113.
[47] Kovasil^{tm} MS Technical Bulletin, Uetikon (1995).
[48] G.Y. Onoda, E. Liniger, Phys. Rev. Lett. 64 (1990) 2727–2730.